

Polymorphism in dithiadiazolyls: A case study of reversible and irreversible phase transitions in *p*-EtOC₆F₄CNSSN.

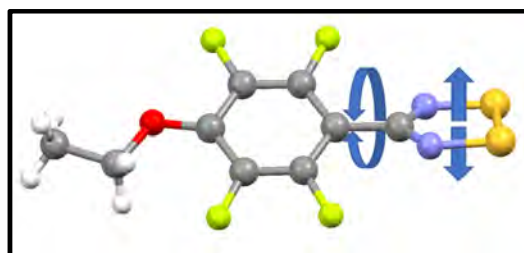
Yassine Beldjoudi,^a Rui Sun,^a Ana Arauzo,^b Javier Campo,^b Robert J. Less^c and Jeremy M. Rawson^{a,c,*}

^a Department of Chemistry & Biochemistry, University of Windsor, 401 Sunset Avenue, Windsor, ON, N9B 3P4, Canada. E-mail: jmrawson@uwindsor.ca

^b Departamento de Física de la Materia Condensada, Facultad de Ciencias, and Instituto de Ciencia de Materiales de Aragon, CSIC-Universidad de Zaragoza, E-50009 Spain.

^c Department of Chemistry, The University of Cambridge, Lensfield Road, Cambridge, UK CB2 1EW

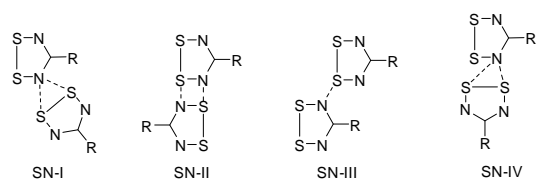
ABSTRACT: The 4'-alkoxy-tetrafluorophenyl dithiadiazolyls, ROC₆F₄CNSSN [R = Me (**1**), Et (**2**), ⁿPr (**3**), ⁿBu(**4**)] all adopt *cis-oid* dimers in the solid state. The methoxy derivative **1** adopts a π -stacked AA'AA' motif whereas propoxy (**3**) and butoxy (**4**) derivatives exhibit an AA'BB' stacking. The ethoxy derivative (**2**) is polymorphic, adopting either an AA'BB' motif (**2 α**) comparable with **3** and **4**, or a structure (**2 β**) more reminiscent of **1** but which combines a mixture of both monomers and dimers in the solid state. The structure of **2 β** is temperature dependent undergoing a phase transition at -25 °C associated with both rotation and translation of the dithiadiazolyl ring. In the high temperature regime (**2 β ₁**) the dimer:monomer ratio is 1:1 but converts to a 3:1 ratio at low temperature (**2 β ₂**). Detailed DSC and variable temperature PXRD studies coupled with SQUID magnetometry have been used to show that **2 α** converts irreversibly to **2 β** upon heating and that **2 β ₁** and **2 β ₂** interconvert through a reversible phase transition with a small thermal hysteresis in its magnetic response.



INTRODUCTION

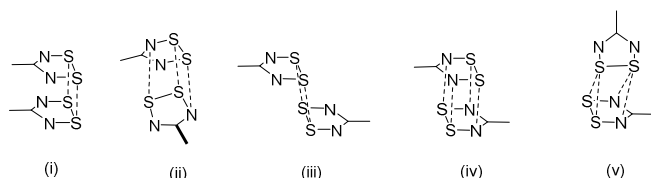
Over the last 30 years 1,2,3,5-dithiadiazolyl (DTDA) radicals have been explored as building blocks for neutral radical conductors,¹ as building blocks in the design of some of the highest T_c organic magnets² and as components in photo-conducting devices.³ They have also been used as ligands in coordination chemistry⁴ and have been shown to undergo oxidative addition to low oxidation state metals.⁵ More recent work have shown that poly-aromatic hydrocarbons bearing a DTDA moiety exhibit photoluminescence.⁶

The electronic properties of 1,2,3,5-dithiadiazolyl (DTDA) radicals such as conductivity and magnetism are heavily dependent on the solid-state structure.⁷ Work by Rawson and Haynes identified common packing motifs between DTDA radicals in the absence of additional functionality (Scheme 1)⁸ and the implementation of other strong structure-directing groups to dictate the structure have been reviewed.⁹ The strong tendency of these radicals to dimerize ($\Delta H_{\text{dim}} \sim 35 \text{ kJ}\cdot\text{mol}^{-1}$)¹⁰ has recently been used by Preuss as a supramolecular synthon for the self-organization of lanthanide-DTDA complexes.¹¹



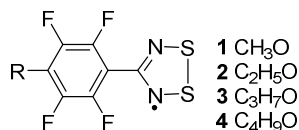
Scheme 1: Common favourable electrostatic in plane S^{δ+}...N^{δ-} contacts identified in DTDA radicals.

The utilisation of DTDA radicals as building blocks for the design of organic magnetic materials necessitates that molecules retain their paramagnetic behavior.⁷ Several strategies have been explored to potentially inhibit the dimerization process. While the presence of sterically demanding substituents can disrupt the common *cis-oid* dimerization (Scheme 2), alternative dimerization modes have been observed. The fine balance between monomer and dimer structures is exemplified by 2,4,6-(F₃C)₃C₆H₂CNSSN which was found to exist in both trans-antarafacial and monomeric forms.¹²



Scheme 2: Common dimerization modes of DTDA radicals: (i) cis-oid, (ii) twisted, (iii) trans-antarafacial, (iv) trans-cofacial and (v) orthogonal configurations.

The most highly implemented approach to suppress dimerization has been the use of perfluoroaryl substituents coupled with structure-directing groups. In these cases, the electrostatic repulsion between the fluorines in the *ortho* position of the perfluoroaryl ring and the nitrogen of the heterocyclic ring leads to a large twist angle (energy minimum at $\theta \sim 50^\circ$)¹³ between the two rings. This makes the perfluoroaryl ring sterically demanding, destabilizing the dimer. In the simplest case, 2,6-F₂C₆H₃CN₂SSN, the compound is found to be trimorphic with two cis dimers formed (tetragonal and monoclinic phases)¹³ and a third monoclinic phase formed which comprises a trans-antarafacial dimer (Scheme 2) and a monomer,¹⁴ reflecting the fine energetic balance between monomer and dimer in this system. In such cases, the inclusion of additional strong structure-directing groups may overcome the tendency for dimerization, exemplified by the presence of CN...S interactions in both α - and β -phases of *p*-NCC₆F₄CN₂SSN^{15,16} as well as *p*-NCC₆F₄C₆F₄CN₂SSN.¹⁷ Similarly NO₂...S interactions in *p*-O₂NC₆F₄CN₂SSN¹⁸ and Br...N sigma-hole interactions in the case of *p*-BrC₆F₄CN₂SSN¹⁹ appear adequate to overcome dimerization. In the current paper, we examine how subtle tuning of the 4'-substituent in the series ROC₆F₄CN₂SSN (R = Me, Et, ⁿPr and ⁿBu, Scheme 3) affects the solid-state structure and probe the polymorphic nature of **2**.



Scheme 3

RESULTS

All four 4-alkoxy perfluoroaryl carbonitrile derivatives, ROC₆F₄CN, were synthesized from a mixture of pentafluorobenzonitrile and sodium alkoxide in the corresponding alcohol based on the literature procedure (see ESI-2).²⁰ The 4'-alkoxy-functionalized perfluoroaryl DTDA radicals **1** – **4** were then prepared using standard synthetic methodologies²¹ using triphenyl antimony as the reducing agent due to the low melting point of the radicals (60 – 80 °C) which avoided any contamination with Ph₃SbCl₂ (mp = 142 °C) during sublimation.²² In this manner radicals **1** – **4** were obtained in crystalline form in 37 – 70 % recovered yield. Radical **2** was found to be polymorphic and necessitated careful monitoring of the temperature of the cold finger in order to selectively crystallize either **2 α** or **2 β** , a procedure that has been already utilised to selectively prepare α - or β -*p*-NCC₆F₄CN₂SSN.¹⁵ In this fashion **2 α** was selectively formed when collected on a cold-finger at -15 °C

whereas **2 β** was isolated when the substrate temperature was maintained at +30 °C.

Crystal structures

Crystallographic data are summarized in Table 1. Radicals **1**, **3** and **4** adopt a single crystalline habit, whereas **2** crystallizes in two different crystalline phases **2 α** and **2 β** .

Table 1: Crystallographic data for **1** – **4**

	1	3	4
Formula	C ₈ H ₃ OF ₄ N ₂ S ₂	C ₁₀ H ₇ OF ₄ N ₂ S ₂	C ₁₁ H ₉ OF ₄ N ₂ S ₂
FW	283.24	311.3	325.3
Temp. (K)	150(2)	173(2)	173(2)
Crystal system	Monoclinic	Monoclinic	Monoclinic
Space group	<i>P</i> 2 ₁ / <i>c</i>	<i>P</i> 2 ₁ / <i>c</i>	<i>P</i> 2 ₁ / <i>c</i>
<i>a</i> /Å	7.3635(4)	16.2391(10)	16.9314(7)
<i>b</i> /Å	31.7443(17)	18.0475(9)	8.0672(3)
<i>c</i> /Å	8.3990(4)	8.1473(5)	22.8387(8)
α /°	90.00	90.00	90.00
β /°	101.436(2)	100.045(2)	124.995(2)
γ /°	90.00	90.00	90.00
<i>V</i> /Å ³	1922.28(17)	2351.2(2)	2555.51(17)
<i>Z</i>	8	8	8
<i>D</i> _c /g·cm ⁻³	1.955	1.759	1.691
<i>R</i> _{int}	0.040	0.055	0.046
<i>R</i> ₁	0.051	0.047	0.043
<i>wR</i> ₂	0.123	0.103	0.099
<i>S</i>	1.15	1.06	1.05
$\Delta\rho_{\max}$, $\Delta\rho_{\min}$ (e Å ⁻³)	0.42, -0.54	0.45, -0.38	0.49, -0.39
	2α	2β₁	2β₂
Formula	C ₉ H ₅ OF ₄ N ₂ S ₂	C ₉ H ₅ OF ₄ N ₂ S ₂	C ₉ H ₅ OF ₄ N ₂ S ₂
FW	297.27	297.27	297.27
Temp. (K)	173(2)	253(2)	173(2)
Crystal system	Monoclinic	Triclinic	Triclinic
Space group	<i>P</i> 2 ₁ / <i>c</i>	<i>P</i> -1	<i>P</i> -1
<i>a</i> /Å	15.6073(15)	8.3271(8)	8.4511(15)
<i>b</i> /Å	17.3379(15)	11.9249(12)	25.774(4)
<i>c</i> /Å	8.1387(7)	35.154(4)	34.955(6)
α /°	90.00	94.5571(7)	90.013(4)
β /°	99.208(5)	91.851(6)	90.207(5)
γ /°	90.00	106.655(6)	94.726(5)
<i>V</i> /Å ³	2173.9(3)	3328.1(6)	7588(2)
<i>Z</i>	8	12	28
<i>D</i> _c /g·cm ⁻³	1.817	1.780	1.822
<i>R</i> _{int}	0.073	0.049	0.096
<i>R</i> ₁	0.077	0.087	0.130
<i>wR</i> ₂	0.170	0.245	0.341
<i>S</i>	1.11	1.02	1.04
$\Delta\rho_{\max}$, $\Delta\rho_{\min}$ (e Å ⁻³)	0.50, -0.45	1.04, -0.45	1.21, -0.80

Selected structure parameters for **1** – **4** are reported in Table 2.

Crystal structure of **1**

Radical **1** crystallises in the space group $P2_1/c$ with one *cis-oid* dimer (two crystallographically independent molecules) in the asymmetric unit. The twist angles between the heterocyclic ring plane and the aryl ring plane for the two molecules are $31.2(5)^\circ$ and $30.8(5)^\circ$, comparable with other perfluorinated aryl DTDA radicals ($14.5 - 57.8^\circ$, mean 37.8°).^{16-19,23} Previous computational studies revealed an energy minimum at $\sim 50^\circ$ but a relatively shallow potential well for deviation away from this minimum such that angles in the range 30 to 90° fall within $3 \text{ kJ}\cdot\text{mol}^{-1}$ of this minimum.¹³ A comparison of the experimentally observed torsion angles for fluorinated and non-fluorinated aryl groups in relation to the computed energies are presented in Fig. S.4.

The intradimer S...S contacts of $3.179(2)$ and $3.198(2) \text{ \AA}$ are shorter than the intra-dimer O...O contact at $3.751(4) \text{ \AA}$ such that the dimer is slightly ‘wedge-shaped’. The angle between the two DTDA planes within the dimer is $\sim 5.6(2)^\circ$. The dimers of **1** adopts a π -stacked structure along the *a*-axis (Figure 1a) in which the inter-dimer S...S contacts ($4.156(2)$ – $4.180(2) \text{ \AA}$) are markedly longer than the intra-dimer S...S distances, like many π -stacked DTDA radicals.^{6,13,24-26} Conversely the inter-dimer O...O distance of $3.615(4) \text{ \AA}$ is comparable with the intra-dimer contact ($3.751(4) \text{ \AA}$) respectively with both significantly longer than twice the van der Waals radii of O (3.04 \AA). Each molecule within a dimer forms close contacts to two neighbouring molecules perpendicular to the stacking direction through electrostatically favorable $\delta^+\text{S}\cdots\text{N}^{\delta-}$ contacts of the SN-IV type (Scheme 1),⁹ leading to a chain-like motif in the *bc*-plane (Figure 1b).

Crystal structures of **2 α** , **3** and **4**

Radicals **2 α** , **3** and **4** crystallize as *cis-oid* dimers in the space group $P2_1/c$, each with two molecules (one dimer) in the asymmetric unit (Fig. 2; Figs. S1 and S2, ESI). The torsion angles between heterocyclic and perfluoroaryl rings in **2 α** , **3** and **4** span the range $29.2 - 44.4(2)^\circ$, comparable

with **1** and other perfluoroaryl DTDA (vide supra).^{16,17,23} Although the intra-dimer S...S contacts ($3.049(1) - 3.206(1) \text{ \AA}$) remain in the typical range for DTDA radicals (Table 2), the intra-dimer O...O separation increases steadily with increasing chain length from $3.751(4)$ to $5.379(2) \text{ \AA}$, revealing a linear relationship between the length of the alkoxy group and O...O separation (Fig. S3 (left), ESI). This increasing O...O separation reflects additional strain through ‘hinging’ at the intra-dimer DTDA S...S contacts with the angle between DTDA ring planes increasing from $5.6(2)$ to $13.3(5)^\circ$ (Table 2).

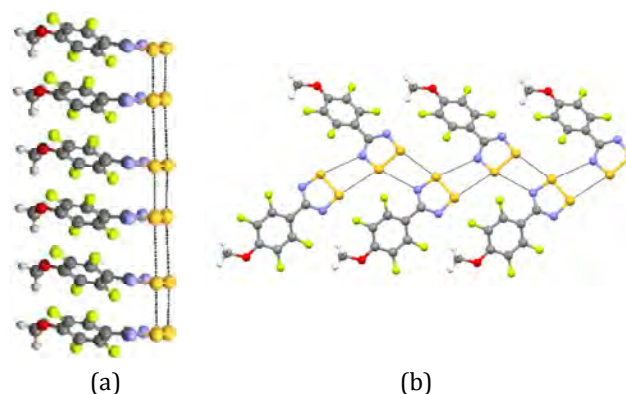


Figure 1: The crystal structure of **1**. (a) π -stacking parallel to the crystallographic *a*-axis; (b) Propagation of inter-stack contacts via SN-IV type interactions in the *bc*-plane.

A consequence of this increased ‘wedging’ of the dimer geometry is to generate a fundamental change in the π -stacking. While **1**, **2 α** , **3** and **4** all crystallise in the $P2_1/c$ space group, the inversion center is located between stacks in **1** (affording an AA’AA’ π -stacking motif) but is positioned within stacks in **2 α** , **3** and **4**, generating an AA’BB’ packing. The latter appears better able to accommodate the more ‘wedge-shaped’ dimers associated with **2 α** , **3** and **4**. The structure of **2 α** is shown in Fig. 2. Perpendicular to the stacking direction **2 α** , **3** and **4** form similar inter-stack contacts to **1** (compare Fig. 1b and Fig 2b).

Table 2: Selected structural parameters for dimers of **1** – **4**

	Intradimer $d_{\text{S}\cdots\text{S}}$ (\AA)	Intradimer $d_{\text{O}\cdots\text{O}}$ (\AA)	Angle between C_6F_4 and DTDA ring planes ($^\circ$)	Angle between DTDA ring planes ($^\circ$)	In plane S...N contacts (\AA)	In plane S...F contacts (\AA)
1	3.179(2)-3.198(2) mean: 3.188	3.751(4)	30.8(5)-31.2(5) mean: 31.0	5.6(2)	3.295(3)- 3.387(3)	3.018(2)-3.232(2)
2α	3.066(2)-3.090(2) mean: 3.078	4.198(4)	29.2(7)-35.3(7) mean: 32.2	8.7(3)	3.102(4)- 3.235(4)	2.990(3)-3.235(3)
2β_1	3.162(8)-3.204(9) mean: 3.183	4.087(4)-4.204(2) mean: 4.145	27(3)-39(3) mean: 33	8.7(4)	3.139(2)- 3.372(2)	3.023(9)-3.220(9)
2β_2	3.124(6)-3.177(6) mean: 3.150	3.877(2)-4.056(2) mean: 3.966	30(2)-36(2) mean: 33	6.3(2)	2.964(3)- 3.324(3)	2.82(3)-3.17(3)
3	3.077(1)-3.137(1) mean: 3.107	4.460(3)	40.0(3)-35.1(3) mean: 37.5	10.0(6)	3.095(2)- 3.247(2)	3.091(1)-3.189(1)
4	3.099(1)-3.049(1) mean: 3.074	5.379(2)	44.4(2)-35.2(2) mean: 39.7	13.3(5)	2.998(1)- 3.236(1)	3.021(1)-3.200(1)

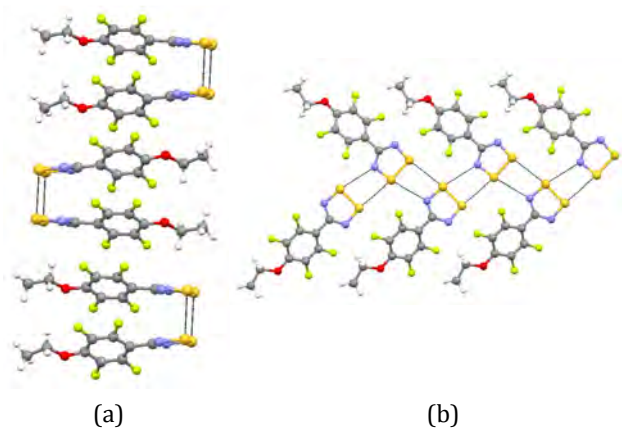


Figure 2: The crystal structure of **2α** (a) Antiparallel arrangement of dimers parallel to the crystallographic *a* axis; (b) Propagation of inter-stack contacts *via* SN-IV type interactions in the *bc*-plane.

In all cases the in-plane S⋯N contacts are supplemented by S⋯F contacts linking dimers together in the *bc* plane. These fall in the range 2.82 – 3.26 Å (Table 2).

The crystal structure of **2β** proved particularly problematic and exhibited a significant temperature dependence. See ESI-4 for a more detailed discussion. Based on DSC data (ESI, Fig. S6) a clear phase transition was apparent around -25 °C and the structure of **2β** was determined above and below this transition temperature. Both phases showed a propensity for twinning and cooling through the phase transition led to significant degradation in crystal quality. The structures described here are the best of multiple crystals examined. In the discussion which follows we will refer to the high temperature phase at -20 °C as **2β₁** and the low temperature structure recorded at -100 °C as **2β₂**.

Crystal structure of **2β₁**

At -20 °C a crystal of **2β** was indexed on a triclinic cell (*P*-1) with 6 molecules in the asymmetric unit. These 6 crystallographically independent molecules comprise two *cis*-oid dimers and two monomeric radicals. The heterocyclic ring planes of the monomers are markedly twisted with respect to the dimer DTDA ring planes (Fig. 3). Structures of DTDA radicals comprising mixtures of both dimers and monomers are rare but not without precedent.^{12,14,27} The intradimer S⋯S contacts fall in the range 3.162(8) – 3.204(9) Å (Table 2) while the corresponding intra-dimer O⋯O separations are 4.087(4) and 4.204(2) Å, comparable with **2α** (4.198(4) Å). The hinge angles between DTDA rings within these dimers are in range 27 – 39 °.

As with other structures in this series, **2β₁** adopts a π -stacked structure parallel to the crystallographic *b*-axis. The two dimers and two monomers in the asymmetric unit form two crystallographically independent stacks with each stack containing one dimer and one monomer (Fig. 3a). Although the perfluoroaryl rings associated with the two monomeric radicals are well-located, their DTDA rings appear thermally disordered (*vide infra*) *via* rotation of the CNSSN ring about the C_{Ar}-C_{DTDA} bond. In each case this

was modelled over two positions. This disorder reveals that there is adequate space between dimers along the stacking direction to accommodate significant DTDA ring rotation in this structure. Notably the major component of disorder in both independent monomers (60% and 85%) reveal the DTDA ring is close to perpendicular to the DTDA rings in the dimers (Fig. 3a). This behaviour is reminiscent of (*o*-ClC₆H₄CN₂SSN)₂ although the latter shows no structural disorder.^{27b} Notably the inter-stack contacts still adopt a similar motif to that observed in the other structures in this series (Fig. 3b). In **2β₁** rotation of 33% of the DTDA rings leads to a mixture of SN-I (two S⋯N contacts with coplanarity unnecessary) and SN-IV (S⋯N and S⋯S contacts between near coplanar DTDA heterocycles). Although the closest centroid...centroid distances between monomers along the stacking direction is 12.4 Å, the two independent rotationally disordered radicals are located adjacent to each other in neighbouring stacks offering an orthogonal π - π interaction between DTDA rings (Fig. 3b). The closest S⋯S contacts in this arrangement are in excess of 3.8 Å, consistent with a van der Waals interaction rather than a π - π interaction between SOMOs.

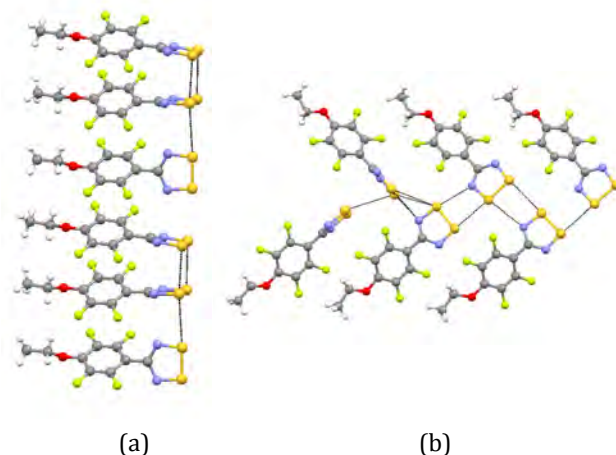


Figure 3: The crystal structure of **2β₁**. (a) One of the two crystallographically independent stacks of dimers and monomers in **2β₁**. (b) Propagation of inter-stack contacts *via* SN-IV and SN-I type interactions.

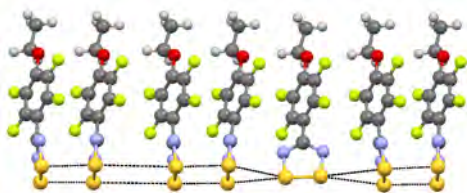
Crystal structure of **2β₂**

On cooling below -25 °C, **2β₁** undergoes a reversible phase transition to **2β₂** which is evident in variable temperature powder X-ray diffraction (VT-PXRD) and DSC studies (*vide infra*). Although samples cooled through the phase transition retained crystallinity, the diffraction pattern persistently reflected some degree of twinning in all crystals examined and was reflected in a poorer internal R value (*R*_{int}) compared to the high temperature phase (Table 1). A full dataset was measured at 173 K (75 K below the phase transition) on a crystal cooled through the phase transition. A distinct change in diffraction profile was evident at low temperature and the new data initially indexed on a higher symmetry monoclinic super-cell. Structure solution in the *P*2₁ space group provided an initial solution with *Z'* = 14 but the refinement stalled at *R*₁ = 27% with evidence

for twinning (systematic observation of $F_o > F_c$ for the most disagreeable reflections). A possible two component twin, close to merohedral was identified but failed to provide a significant improvement in R_1 . When the data were reprocessed in the lower symmetry triclinic setting, a similar solution in $P-1$ ($Z' = 14$) was identified. In this case application of the merohedral twin law $(-1\ 0\ 0\ -1\ 0\ 0\ 0\ 0\ 1)$ led to a marked decrease in R_1 and refinement proceeded smoothly to afford a final R_1 of 13%. Although the R value is high it is in line with the intrinsic quality of the data ($R_{int} \sim 9\%$) and linked to the inherent degradation in crystal quality on passing through the phase transition. Attempts to grow single crystals of this low temperature phase directly by using a low temperature cold finger proved unsuccessful due to the thermodynamic preference to crystallise **2 α** at these lower temperatures.

The unit cell parameters of **2 β_2** are similar to those of **2 β_1** but with an expansion of the crystallographic b axis and some modification of the unit cell angles. The structure of **2 β_2** contains 14 molecules in the asymmetric unit, three of which show a small degree of disorder ($< 10\%$) in the orientation of the DTDA ring. Considering only the major component of the disorder then the low temperature structure comprises 6 *cis*-oid dimers and two monomers which can be split into two crystallographically independent stacks, each containing three dimers and a monomer (Fig. 4a).

(a)



(b)

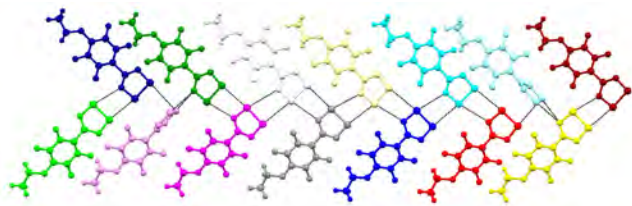


Figure 4: The crystal structure of **2 β_2** . (a) One of the two crystallographically independent stacks of dimers and monomers; (b) Propagation of inter-stack contacts via SN-IV and SN-I type interactions (molecules coloured by crystallographic independence).

In **2 β_1** the structure comprised an alternating dimer-monomer repeat along the stacking direction (Fig. 3a) whereas **2 β_2** now exhibits a repeat unit of three dimers and a monomer along the stacking direction (Fig 4a). The combination of the 3 molecule repeat for **2 β_1** and 7 molecule repeat for **2 β_2** requires a common super-cell containing 21 molecules along the stacking direction. As a consequence, the transition from **2 β_1** to **2 β_2** requires disruption of both the existing dimers as well as monomers becoming involved in dimer formation. A representation of the dis-

placement of the radicals in **2 β_1** and **2 β_2** along the stacking direction in relation to the supercell is presented in Fig. 5. Given the disruption along the stacking direction associated with the phase transition, it is perhaps unsurprising that there was an inherent decrease in crystal quality on passing through this phase transition. As with **2 β_1** , the monomeric radicals in **2 β_2** exhibit some rotational disorder although this is much reduced when compared to **2 β_1** . In **2 β_2** monomers are not only well isolated along the stacking direction (monomer...monomer separation ~ 28 Å) but also between stacks (monomer...monomer separation ~ 13 Å). Between stacks the radicals are once again linked *via* a combination of SN-I and SN-IV type contacts (Fig. 4b).

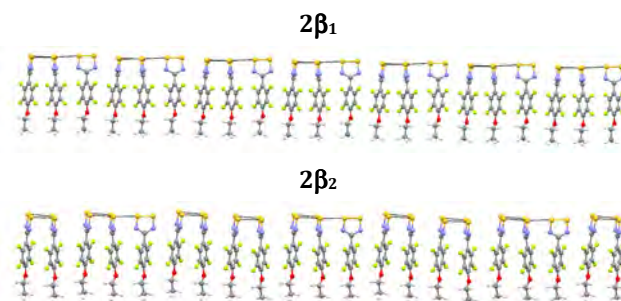


Figure 5: Comparison of the common supercell associated with π -stacking in **2 β_1** (top) and **2 β_2** (bottom)

Comparison of structures of 1 – 4

DTDA radicals bearing simple phenyl ring substituents often adopt herringbone motifs through $\delta^+S \dots \pi$ interactions as exemplified by $(PhCNSSN)_2$.²⁸ The inclusion of the perfluoroaryl group reduces π -spin density evidenced by Haynes' charge density studies on $(PhCNSSN)_2$, and $(C_6F_5CNSSN)_2$,²⁹ suppressing herringbone motifs in these perfluoro-aryl DTDA. ^{16-19,23} Their heavier Se analogues³⁰ also tend to adopt π -stacked/layer-like structures. The structures of **1** – **4** all comprise *layer-like* architectures which maximize inter-stack $S \dots N$ contacts of the type SN-I and SN-IV (Figs. 1b, 2b, 3b, 4b and ESI. Figs. S1b, S2b). The arrangement of molecules along the stacking direction appears sensitive to the functional group size. While compounds **1**, **2 β_1** and **2 β_2** adopt π -stacked structures (of the AA'AA' variety), **2 α** , **3** and **4** adopt layered structures in which discrete dimers align antiparallel adopting an AA'BB' motif. The former appears stabilized through dispersion and weak inter-dimer bonding interactions whereas the latter is stabilized through dipole-dipole interactions. The increase of the alkyl chain length affords a linear increase of the unit cell volume (Fig. S4 (right)) and a monotonic increase in O...O separation within dimers, affording a more 'wedge-shaped' motif for larger alkyl groups. This subtle change in geometry of the *cis*-oid dimers leads to marked changes in the solid-state packing. While the smaller methoxy derivative **1** forms a π -stacked structure, the larger alkoxy derivatives (**3** and **4**) which exhibit more wedge-shaped geometries adopt AA'BB' motifs as a more efficient packing mode (Fig 6). In the case of **2** there is a fine balance between these two scenarios with polymorph **2 β** exhibiting the AA'AA' motif and **2 α** reveal-

ing an AA'BB' stacking pattern. In $2\beta_1$ and $2\beta_2$ the AA'AA' packing of the wedge-shaped motif leads to some degree of inefficient packing. At low temperature ($2\beta_2$) one radical defect is observed for every three dimers but thermal expansion of the lattice leads to additional monomers at elevated temperatures ($2\beta_1$ exhibits one monomer per dimer) enhancing the number of 'paramagnetic defects' in the lattice on warming.

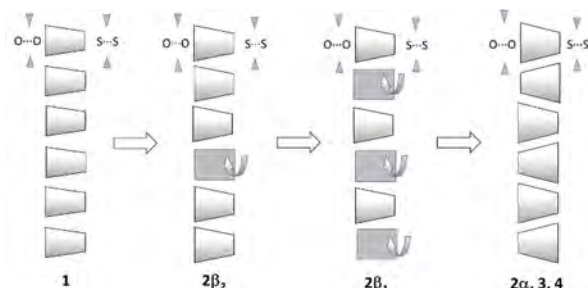


Figure 6: Packing arrangements for **1** – **4**. Trapezoids represent dimers and rectangles represent rotationally disordered monomers.

Thermal studies on **1** – **4**

A summary of the thermodynamic data determined from DSC studies for **1** – **4** is presented in Table S2 and values quoted in the text refer to onset temperatures (T_{onset}). DSC studies on **1** and **4** revealed the presence of a single endothermic process at 78 °C and 58 °C for **1** and **4** respectively associated with their melting points.

The selective preparation of both polymorphs 2α and 2β permitted a series of studies on the relative stabilities and phase transitions of **2**. For 2α variable temperature single crystal and powder X-ray diffraction studies showed no significant structure change in 2α from -170 to +65 °C (Fig. 6a). At 75(2) °C PXRD studies revealed 2α had converted to $2\beta_1$ (Fig. 6a). DSC studies on a pure sample of 2α revealed the presence of two successive endothermic transitions on warming at +76 and +80 °C with a total enthalpy change of $\Delta H = +20 \text{ kJ}\cdot\text{mol}^{-1}$ on the heating cycle (ESI, Fig. S6). The first transition is attributed to the conversion of 2α to $2\beta_1$ whilst the second is attributed to the melt of $2\beta_1$. Upon slow cooling, recrystallization of liquid **2** occurs with formation of $2\beta_1$, confirmed by VT-PXRD studies (Fig. 7). A comparison of the structures of 2α to $2\beta_1$ reveal that the transformation of 2α to $2\beta_1$ requires a major lattice reorganisation (50% of molecules to undergo a 180° rotation or 100% of molecules to undergo a 90° rotation). Previous studies have identified such major lattice reorganizations occur *via* a melt/recrystallization process.¹⁵ The endothermic nature of the conversion of 2α to 2β indicates this spontaneous process is entropically driven such that 2α is the thermodynamically preferred of the two polymorphs and 2β is the entropically more stable phase. Based on the density rule,³¹ ($2\alpha = 1.842 \text{ g}\cdot\text{cm}^{-3}$ cf $2\beta_1 = 1.781 \text{ g}\cdot\text{cm}^{-3}$) the lattice enthalpy of 2α is greater than $2\beta_1$ in agreement with these experimental observations.

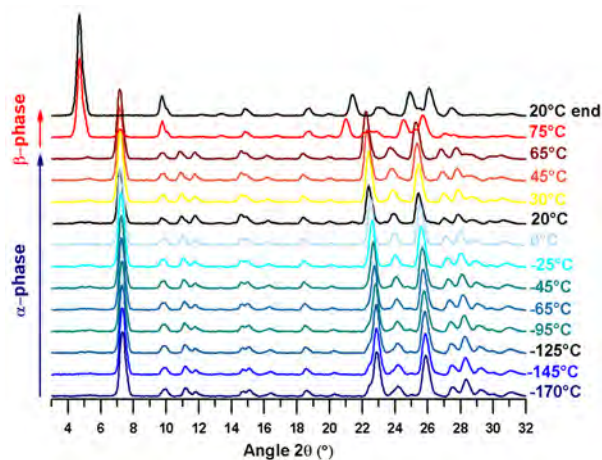


Figure 7: Variable temperature PXRD profiles observed on heating 2α .

DSC studies on a pure sample of 2β heated from -60 to +150 °C revealed two endothermic transitions occurring at -25 °C and +78 °C. The transition at -25 °C is associated with the phase transition from the low temperature phase $2\beta_2$ to the high temperature phase $2\beta_1$, corroborated by single crystal and PXRD studies (Fig. 8). The enthalpy change associated with this process ($+0.6 \text{ kJ}\cdot\text{mol}^{-1}$) is extremely small. The transition at +78 °C ($\Delta H_{\text{fus}} = +19.2 \text{ kJ}\cdot\text{mol}^{-1}$) is assigned to the melting of $2\beta_1$. On cooling a small transition at -30 °C was recorded reflecting the reversible nature of the $2\beta_2$ to $2\beta_1$ transition. This behaviour was confirmed by VT-PXRD studies (Fig. 8) which revealed the disappearance of weak reflections around 7° and 16° as well as a more intense feature near 22°/2θ on cooling to -25 °C. More subtle changes in peak position and intensities were evident on cooling from -25 °C to -170 °C, suggestive of a dynamic process in this regime. In addition the re-emergence of the original PXRD profile on warming back to room temperature confirmed the reversible nature of the $2\beta_1 \leftrightarrow 2\beta_2$ transition seen in DSC studies. Powder patterns for $2\beta_1$ and $2\beta_2$ were in good agreement with those predicted from the single crystal X-ray data.

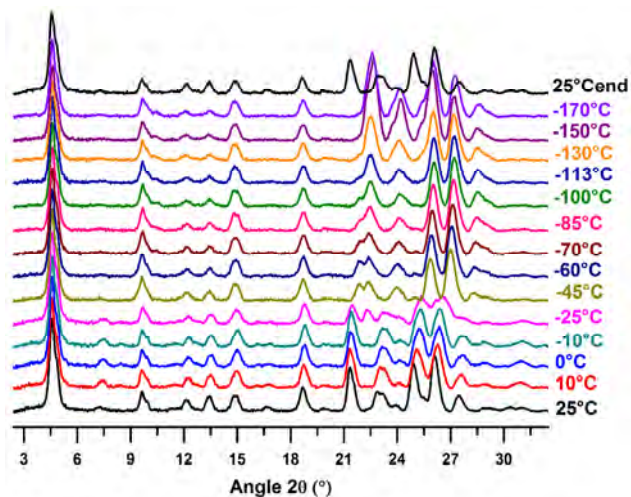


Figure 8: Variable temperature PXRD profiles of $2\beta_1$ on cooling

Application of the density rule ($2\beta_1 = 1.781 \text{ g.cm}^{-3}$, cf $2\beta_2 = 1.821 \text{ g.cm}^{-3}$) suggests that the lattice enthalpy of $2\beta_2$ is greater than that of $2\beta_1$ and therefore the conversion of $2\beta_2$ to $2\beta_1$ on warming is entropically driven, consistent with the increasing number of disordered monomers. In this context, $2\beta_1$ can be considered as the most entropically favourable phase whereas 2α is the most enthalpically favourable phase with $2\beta_2$ metastable in the low temperature region. This is entirely consistent with experimental observations that sublimation at high temperature (substrate temperature +30 °C) affords selectively the most entropically favourable phase $2\beta_1$ whereas sublimation using low substrate temperatures (-15 °C) affords the most enthalpically stable phase (2α) with $2\beta_2$ only isolated through the solid-state transformation $2\beta_1 \rightarrow 2\beta_2$ on cooling.

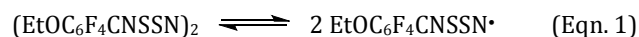
Radical **3** reveals two endothermic transitions on heating ($T_{\text{onset}} = 64$ and 91 °C). VT-PXRD studies on **3** reveal no significant change in the profile of the powder pattern across the temperature range $20 - 65$ °C, agreeing well with that predicted based on the single crystal structure determination (Fig. S9, ESI). At 80 °C, the pattern changed significantly to afford just a few broad low intensity features. We tentatively assign this to the formation of a glassy phase with some degree of structural order (possibly a liquid crystalline phase). The second transition at 91 °C has a much lower enthalpy change ($\Delta H = 1.54 \text{ kJ.mol}^{-1}$) consistent with the breakdown of the final components of short range ordering and formation of an isotropic liquid. The integrity of the radical over this temperature range was confirmed by the VT-PXRD studies which revealed reformation of crystalline **3** upon cooling (see Fig. S9, ESI).

Magnetic studies on 2α and 2β

DC magnetic studies on 2α and 2β were measured on a Quantum Design SQUID magnetometer. Data for 2α (69 mg) were measured from 5 to 300 K with the sample sealed in a gelatin capsule with an applied field of 10000 Oe. The sample of 2β (47 mg) was mounted in a quartz tube and measured from 150 to 375 K with an applied field of 10000 Oe. Additional heating and cooling cycles on 2β (46 mg) mounted in a gelatin capsule were undertaken in applied fields of 500 Oe. Data were corrected for diamagnetism of the sample and holder.

For 2α , the value of χT remains approximately constant at $0.003 \text{ emu}\cdot\text{K}\cdot\text{mol}^{-1}$ on warming up to 250 K (Fig 8a), consistent with a small number of $S = \frac{1}{2}$ defects in the crystal lattice (0.6%). Above 250 K the susceptibility of 2α begins to increase. The onset of significant sample paramagnetism in such DTDA dimers has been reported for a number of DTDA radicals and has previously been shown to be consistent with thermal population of a low-lying excited state triplet.^{25,26,32} In the current case, modelling the magnetic data to the Bleaney-Bowers model³³ [$H = -2/S_1\cdot S_2$] failed to reproduce the sample paramagnetism (Fig. 9(top)). Alternatively paramagnetism may arise from some degree of dissociation of the dimers to form monomers in the solid state. Similar arguments have been implemented to model the low paramagnetism observed in the liquid phase of F_3CCNSSN .³⁴ In this context, we applied a simple monomer-

dimer equilibrium model (Eqn. 1) based on a two parameter fit (ΔH_{dim} and ΔS_{dim}) which define the percentage monomer present (see ESI-9).



This behaviour is not unreasonable within the context of the recent pair exchange dynamics model proposed for related thiazyl radicals (*vide infra*).³⁵ This dimer dissociation model assumes that both exchange coupling (i) between the two radicals generated and (ii) to neighbouring radicals is negligible. At low temperature when the equilibrium lies far to the left (Eqn. 1) then the small numbers of monomer pairs generated are well separated from each other. The latter is certainly a good assumption. The assumption that exchange coupling between radical pairs generated by dimer dissociation is negligible should be treated more cautiously, although computed exchange couplings between radicals at/near the sum of the van der Waals radii are typically an order of magnitude or more less ($< 10^2$ K) than the intra-dimer exchange coupling.³⁶

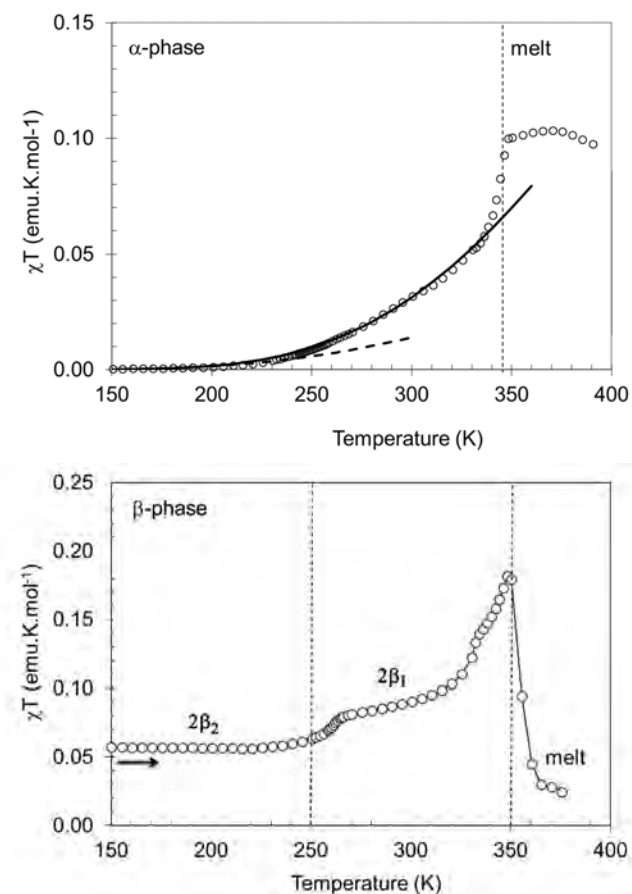


Figure 9: Plots of χT vs T for 2α (top) and 2β (bottom). For 2α , the dashed line corresponds to the fit to the Bleaney-Bowers model whereas the solid line corresponds to the dimer model. For 2β the solid line merely acts as a guide to the eye.

Neglecting the possibility of radical-radical exchange coupling, the magnetic data of **2 α** can be well fitted to the equilibrium model with just two parameters. The values of ΔH_{dim} ($-30 \text{ kJ}\cdot\text{mol}^{-1}$) and ΔS_{dim} ($-71 \text{ J}\cdot\text{K}^{-1}\cdot\text{mol}^{-1}$) are gratifyingly comparable with experimentally determined ΔH_{dim} and ΔS_{dim} values for $(\text{PhCNSSN})_2$ in solution ($\Delta H_{\text{dim}} = -35 \text{ kJ}\cdot\text{mol}^{-1}$, $\Delta S = -121 \text{ J}\cdot\text{K}^{-1}\cdot\text{mol}^{-1}$).^{10b} A surge in the value of χT commences around 340 K and levels off at 350 K and is associated with the melting of **2 α** to form liquid **2**.

For **2 β** , the low temperature value of χT remains constant at $0.057 \text{ emu}\cdot\text{K}\cdot\text{mol}^{-1}$ up to 250 K (Fig. 9), close to the value expected for 1-in-7 radicals being unpaired ($0.054 \text{ emu}\cdot\text{K}\cdot\text{mol}^{-1}$), consistent with the structural data for **2 β_2** . From 246 to 264 K there is a step in the value of χT , increasing to $0.089 \text{ emu}\cdot\text{K}\cdot\text{mol}^{-1}$, a little less than that predicted for one third of the molecules contributing to sample paramagnetism ($0.125 \text{ emu}\cdot\text{K}\cdot\text{mol}^{-1}$) anticipated from the structure of **2 β_1** . From 330 to 350 K there is a further increase in paramagnetism up to a maximum of $0.180 \text{ emu}\cdot\text{K}\cdot\text{mol}^{-1}$ as the sample approaches the melting point, corresponding to ca. 50% unpaired spins. This behavior is comparable with other studies on DTDA radicals in the liquid phase where the value of χT remains below the value expected for a pure $S = \frac{1}{2}$ system and has been attributed to aggregation in the melt.³⁴ The final decrease in χT above the melting point is associated with loss of sample from the cavity space through sublimation and reflected in coating of the quartz sample holder with radical when removed from the magnetometer. Additional studies of the phase transition **2 β_1** \leftrightarrow **2 β_2** in heating and cooling modes confirm the reversible nature of the transition and presence of a small thermal hysteresis loop. If the onset temperatures for the phase transition on heating/cooling are considered then there is negligible hysteresis ($T_c = 257(1) \text{ K}$) but if the transition temperatures are defined by the maximum change in gradient of $\chi T(T)$ then this affords ($T_{c(\uparrow)} = 261(1) \text{ K}$, $T_{c(\downarrow)} = 256(1) \text{ K}$) (scan rate = $1 \text{ K}\cdot\text{min}^{-1}$) (Fig. 10). Additional heat capacity measurements (scan rate = $0.1 \text{ K}\cdot\text{min}^{-1}$) agree well with the SQUID data, affording a peak maximum at 259 K.

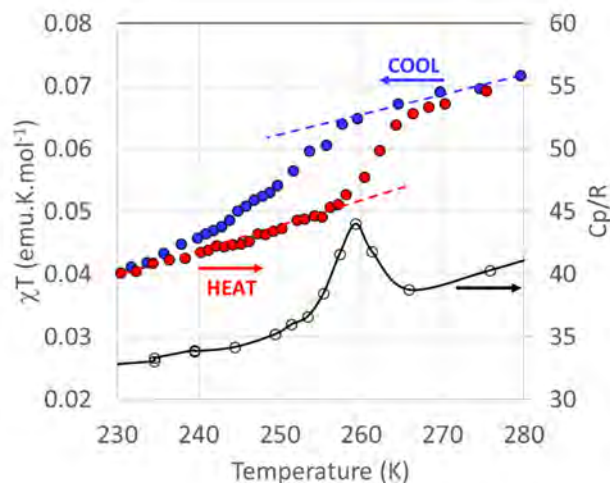


Figure 10: Plot of χT vs T on heating and cooling for **2 β** and the heat capacity measured over the same temperature range. The dotted and solid lines merely act as a guide to the eye.

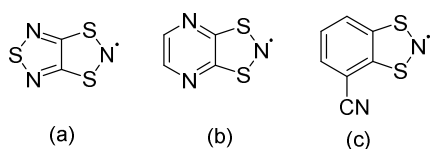
DISCUSSION

The broad family of thiazyl radicals exhibit a rich tapestry of polymorphism and structural transitions which are often reflected in variously subtle or remarkable changes to their solid-state properties (magnetism and transport behaviour).⁷ Polymorphism in DTDA is manifested in different modes of dimerization and/or different solid-state packing motifs. Even ‘simple’ radicals such as HCNSSN³⁷ and ClCNSSN^{8,38} where the molecules are completely rigid have been found to be polymorphic. For example ClCNSSN exhibits two *cis-oid* dimer forms (α and γ -polymorphs) and three twisted dimer forms (β , δ and ϵ -polymorphs) reflecting small energetic differences between *cis-oid* and *twisted* dimer conformations as well as subtle nuances in molecular packing.^{8,38} The two polymorphs of 2',4',6'-(CF₃)₃C₆H₂CNSSN and three polymorphs of 2',6'-F₂C₆H₃CNSSN reveal the subtle balance between both monomeric and dimeric structures,^{12,14} with the latter exhibiting two dimeric forms (both *cis-oid* dimers)¹³ and one phase containing a mixture of both monomers and trans-antarafacial dimers.¹⁴ Despite the many examples of polymorphism in DTDA chemistry, few studies have probed the relative stability of the two phases.^{15,21} A notable exception is the monomeric radical *p*-NCC₆F₄CNSSN which crystallises as either of two polymorphs depending upon sublimation conditions. Recent studies revealed this radical undergoes an irreversible conversion of the α to β polymorphs through a melt-recrystallization process.¹⁵ DSC studies were in agreement with the α -phase being the enthalpically more stable phase (isolated by sublimation at low temperature) and the β -phase being the entropically favoured phase.

In this paper, we find that radical **2** is trimorphic with **2 α** the enthalpically favoured phase, formed during crystallisation at low temperature with **2 β** crystallising selectively at high temperature. The polymorphism in **2** appears to arise as a result of its structural intermediary between **1** which adopts an AA'AA' stacked structure and both **3** and **4** which adopt an AA'BB' stacking.

The significant structural differences between **2 α** and **2 β** are reflected in a melt-recrystallisation process for the irreversible endothermic **2 α** \rightarrow **2 β_1** transformation. While the evident instability in **2 β_1** on cooling cannot be alleviated by a **2 β_1** \rightarrow **2 α** transformation, an alternative metastable state **2 β_2** is observed which is more enthalpically favourable than **2 β_1** . This is formed through a reversible solid-state phase transition, associated with a complex cascade type mechanism in which there are subtle molecular displacements and ring rotations along the stacking direction (Fig. 5). Notably both **2 β_1** and **2 β_2** contain different ratios of monomers and dimers and so the phase transition exhibits an associated (albeit subtle) change in magnetic response. Such structural changes are not without precedent in thiazyl radical chemistry, although the behaviour of **2 β** appears unique in that it combines both rotations and displacements of the thiazyl ring. In both the current case and the 2-chloro-5-halo-phenyl dithiadiazolyl radicals,²⁶ it would appear that the aryl substituents provide a well-defined framework of near-regular displacements along the stacking direction which are mis-matched

with the preferred DTDA stacking interactions. This motif would appear to support dynamic behaviour along the stacking direction. Within the family of 1,3,2-dithiazolyls (which exhibit a weak dimerization enthalpy), similar displacive transitions have been reported for π -stacked DTDA radicals, exemplified by 1,3,5-trithia-2,4,6-triazapentalenyl (TTTA),³⁹ 1,3,2-dithiazolo[4,5-*b*]pyrazin-2-yl (PDTA)⁴⁰ and 3-cyanobenzo-1,3,2-dithiazolyl (NCBDTA) *inter alia* (Scheme 4).⁴¹ In the case of TTTA and PDTA these transitions show significant thermal hysteresis associated with the cleavage of inter-stack contacts.⁴² Studies by Novoa *et al.*³⁵ using a combination of *ab initio* molecular dynamics simulations and X-ray measurements, have revealed that the origin of the regular π -stacked motif of the high temperature polymorph of TTTA arises as a result of fast intra-stack pair-exchange dynamics in which displacive motion of the radicals along the stacking direction plays a key role in driving the phase transition.



Scheme 4: (a) 1,3,5-trithia-2,4,6-triazapentalenyl (TTTA) (b) 1,3,2-dithiazolo[4,5-*b*]pyrazin-2-yl (PDTA) (c) 3-cyanobenzo-1,3,2-dithiazolyl (NCBDTA)

The nearest structural transitions which resemble that in **2 β** are the behaviour reported for the biphenyl-substituted dithiadiazolyl radicals^{27a,43} and the first order transitions associated with a lanthanide-bridging DTDA complex described by Preuss.^{11b} The latter exhibits two sequential structural phase transitions at 160 and 310K which involve rupture of 50% (160 K) and 100% (310 K) of the DTDA π^* - π^* dimer interactions. Further studies on the structural and magnetic properties of π -stacked DTDA radicals are ongoing in our laboratory.

CONCLUSIONS

The length of the alkoxy chain influences the solid-state structures of the alkoxy-tetrafluorophenyl DTDA radicals **1** – **4** in a systematic fashion. The ethoxy derivative **2** appears to be at the crossing point in terms of structure stability and was found to be polymorphic; **2 α** adopts the AA'BB' dimer motif observed for **3** and **4** whereas **2 β** adopts a cofacial packing arrangement akin to **1**. Unlike **1**, the structure of **2 β** is more complex with the structure seemingly unable to support formation of a pure dimer phase. At low temperature, the structure of **2 β_2** comprises a 3:1 ratio of dimers to monomers, whereas the high temperature the dimer:monomer ratio is 1:1. The rich polymorphism and phase transition behaviour associated with **2** was probed by DSC, VT-PXRD and SQUID magnetometry. These reveal an irreversible transition from **2 α** to **2 β** upon warming and a reversible transition between high and low temperature forms of **2 β** which are associated with a unique dynamic process along the stacking direction involving both displacive and rotational motion of the DTDA radicals.

ASSOCIATED CONTENT

Supporting Information

The Supporting Information is available free of charge on the [ACS Publications website](#) at DOI:

Experimental details of the preparation of the starting nitriles, ROC₆F₄CN and radicals **1** – **4**; Variable temperature DSC and PXRD studies on both **2 α** and **2 β** ; Crystallographic details of the data collection, processing and refinement for **1** – **4**. Details of the magnetic measurements on **2**. Crystal structures of **1** – **4** including variable temperature structural studies on **2 α** (103–268 K) in cif format.

AUTHOR INFORMATION

Corresponding Author

* jmrawson@uwindsor.ca

Present Addresses

† Department of Chemistry and Chemical Biology, Harvard University, 12 Oxford Street, Cambridge, MA 02138, United States.

Author Contributions

The manuscript was written through contributions of all authors. / All authors have given approval to the final version of the manuscript. / ‡These authors contributed equally. (match statement to author names with a symbol)

Notes

The structure of **1** – **4** have been deposited with the CCDC (deposition numbers 1565879 – 1565888).

ACKNOWLEDGMENT

We would like to thank NSERC and the Canada Research Chairs Program for financial support (J.M.R.), the University of Windsor for a scholarship (Y.B.) and C.F.I./O.R.F. support for infrastructure. We thank the Inorganic Chemistry Exchange (I.C.E.) Program for the opportunity for R.S. to visit U. Windsor. We also acknowledge support from the Ministerio de Economía y Competividad of Spain and the European Regional Development Fund. Additional support from Diputación General de Aragón (DGA-M4) is also acknowledged. (J.C. and A.A)

REFERENCES

- (1) Bryan, C. D.; Fleming, R. M.; Glarum, S. H.; Haddon, R. C.; Oakley, R. T.; Palstra, T. T. M.; Perel, A. S.; Schneemeyer, L. F.; Waszczak, J. V.; Cordes, A. W. *Nature* **1993**, *365*, 821.
- (2) Thomson, R. I.; Pask, C. M.; Lloyd, G. O.; Mito, M.; Rawson, J. M. *Chem. Eur. J.* **2012**, *18*, 8629.
- (3) Iwasaki, A.; Hu, L.; Suizu, R.; Nomura, K.; Yoshikawa, H.; Awaga, K.; Noda, Y.; Kanai, K.; Ouchi, Y.; Seki, K.; Ito, H. *Angew. Chem. Int. Ed. Engl.* **2009**, *48*, 4022.
- (4) (a) Preuss, K. E. *Dalton Trans.* **2007**, 2357. (b) Preuss, K. E. *Coord. Chem. Rev.* **2015**, *289*, 45. (b) Lau, H. F.; Ng, V. W. L.; Koh, L. L.; Tan, G. K.; Goh, L. Y.; Roemmele, T. L.; Seagrave, S. D.; Boéré, R. T. *Angew. Chem., Int. Ed.* **2006**, *45*, 4498.
- (5) (a) Banister, A. J.; May, I.; Rawson, J. M.; Smith, J. N. B. *J. Organomet. Chem.* **1998**, *550*, 241. (b) Banister, A. J.; Gorrell, I.

- B.; Clegg, W.; Jørgensen, K. A. *J. Chem. Soc. Dalton Trans.* **1989**, 2229.
- (6) (a) Beldjoudi, Y.; Osorio-Roman, I.; Nascimento, V.; Rawson, J. M.; *J. Mater. Chem.C* **2017**, *5*, 2794. (b) Beldjoudi, Y. PhD Thesis, University of Windsor, **2016**.
- (7) Rawson, J. M.; Alberola, A.; Whalley, A. *J. Mater. Chem.* **2006**, *16*, 2560.
- (8) Bond, A.D.; Haynes, D. A.; Pask, C.M.; Rawson, J. M. *J. Chem. Soc., Dalton Trans.* **2002**, 2522.
- (9) Haynes, D. A. *CrystEngComm*, **2011**, *13*, 4793.
- (10) (a) Brooks, W.V.F.; Burford, N.; Passmore, J.; Schriver, M.J.; Sutcliffe, L.H. *J.C.S. Chem. Commun.* **1987**, 69; (b) Fairhurst, S. A.; Johnson, K. M.; Sutcliffe, L. H.; Preston, K. F.; Banister, A. J.; Hauptman, Z.V.; Passmore, J. *J. Chem. Soc. Dalton Trans.*, **1986**, 1465.
- (11) (a) Fatila, E. M.; Maahs, A. C.; Mills, M. B.; Rouzières, M.; Soldatov, D. V.; Clérac, R.; Preuss, K. E.; *Chem. Commun.* **2016**, 52, 5414. (b) Fatila, E. M.; Mayo, R. A.; Rouzières, M.; Jennings, M. C.; Dechambenoit, P.; Soldatov, D. V.; Mathonière, C.; Clérac, R.; Coulon, C.; Preuss, K. E. *Chem. Mater.* **2015**, *27*, 4023.
- (12) Alberola, A.; Clarke, C. S.; Haynes, D. A.; Pascu, S. I.; Rawson, J. M. *Chem. Commun.* **2005**, 4726.
- (13) Clarke, C. S.; Haynes, D. A.; Smith, J. N. B.; Batsanov, A. S.; Howard, J. A. K.; Pascu, S. I.; Rawson, J. M. *CrystEngComm*, **2010**, *12*, 172.
- (14) Fatila, E. M.; Jennings, M. C.; Goodreid, J.; Preuss, K. E. *Acta Cryst. C* **2010**, *66*, 260.
- (15) Beldjoudi, Y.; Arauzo, A.; Palacio, F.; Pilkington, M.; Rawson, J. M. *J. Am. Chem. Soc.*, **2016**, *138*, 16779.
- (16) (a) Banister, A. J.; Bricklebank, N.; Clegg, W.; Elsegood, M. R. J.; Gregory, C. I.; Lavender, I.; Rawson, J. M.; Tanner, B. K. *J. Chem. Soc., Chem. Commun.* **1995**, 679. (b) Banister, A. J.; Bricklebank, N.; Lavender, I.; Rawson, J. M.; Gregory, C. I.; Tanner, B. K.; Clegg, W.; Elsegood, M. R. J.; Palacio, F. *Angew. Chem., Int. Ed.*, **1996**, *35*, 2533.
- (17) Alberola, A.; Less, R. J.; Palacio, F.; Pask, C. M.; Rawson, J. M. *Molecules* **2004**, *9*, 771.
- (18) Alberola, A.; Less, R. J.; Pask, C. M.; Rawson, J. M.; Palacio, F.; Oliete, P.; Paulsen, C.; Yamaguchi, A.; Farley, R. D.; Murphy, D. M. *Angew. Chem., Int. Ed.* **2003**, *42*, 4782.
- (19) Antorrena, G.; Davies, J. E.; Hartley, M.; Palacio, F.; Rawson, J. M.; Smith, J. N. B.; Steiner, A. *Chem. Commun.* **1999**, 1393.
- (20) (a) Kyoichi, T.; Hideki, S.; Patent No JP 06145129, May 24, **1994**. (b) Birchall, J. M.; Haszeldine, R. N.; Jones, M. E. *J. Chem. Soc. C*, **1971**, 1343.
- (21) Robinson, S. W.; Haynes, D. A.; Rawson, J.M. *CrystEngComm*, **2013**, *15*, 10205.
- (22) (a) Boéré, R. T. *CrystEngComm*, **2016**, *18*, 2748; (b) Mills, M. B.; Hollingshead, A. G.; Maahs, A. C.; Soldatov, D. V.; Preuss, K. E. *CrystEngComm*, **2015**, *17*, 7816.
- (23) (a) Allan, C.; Haynes, D. A.; Pask, C. M.; Rawson, J. M.; *CrystEngComm*, **2009**, *11*, 2048. (b) Domagała, S.; Haynes, D. A.; *CrystEngComm*, **2016**, *18*, 7116.
- (24) (a) Banister, A. J.; Batsanov, A. S.; Dawe, O. G.; Herbertson, P. L.; Howard, J. A. K.; Lynn, S.; May, I.; Smith, J. N. B.; Rawson, J. M.; Rogers, T. E.; Tanner, B. K.; Antorrena, G.; Palacio, F. *J. Chem. Soc. Dalton Trans.* **1997**, 2539. (c) Bell, A. M. T.; Smith, J. N. B.; Atfield, J. P.; Rawson, J. M.; Shankland, K.; David, W. I. F. *New J. Chem.* **1999**, *23*, 565.
- (25) (a) Constantinides, C. P.; Eisler, D. J.; Alberola, A.; Carter, E.; Murphy, D. M.; Rawson, J. M. *CrystEngComm*, **2014**, *16*, 7298.
- (26) Constantinides, C. P.; Carter, E.; Eisler, D.; Beldjoudi, Y.; Murphy, D. M.; Rawson, J. M. *Cryst. Growth Des.* **2017**, *17*, 3017.
- (27) (a) Barclay, T. M.; Cordes, A. W.; George, N. A.; Haddn, R. C.; Itkis, M. E.; Oakley, R. T.; *Chem. Comm.*, **1999**, 2269; (b) Alberola, A.; Carter, E.; Constantinides, C. P.; Eisler, D. J.; Murphy, D. M.; Rawson, J. M. *Chem. Comm.* **2011**, 47, 2532.
- (28) Vegas, A.; Pérez-Salazar, A.; Banister, A. J.; Hey, R. G. *J. Chem. Soc., Dalton Trans.* **1980**, 1812.
- (29) Domagała, S.; Kosc, K.; Robinson, S. W.; Haynes, D. A.; Woźniak, K. *Cryst. Growth Des.* **2014**, *14*, 4834.
- (30) (a) Feeder, N.; Less, R. J.; Rawson, J. M.; Oliete, P.; Palacio, F. *Chem. Commun.* **2000**, 2449; (b) Melen, R. L.; Less, R. J.; Pask, C. M.; Rawson, J. M. *Inorg. Chem.*, **2016**, *55*, 11747.
- (31) (a) Burger, A.; Ramberger, R. *Mikrochim. Acta.* **1979**, *2*, 273. (b) Burger, A.; Ramberger, R. *Mikrochim. Acta.* **1979**, *2*, 259.
- (32) Shuvaev, K. V.; Decken, A.; Grein, F.; Abedin, T. S. M.; Thompson, L. K.; Passmore, J. *Dalton Trans.* **2008**, 4029.
- (33) Bleaney, B.; Bowers, K.D. *Proc. R. Soc. A* **1952**, *214*, 451.
- (34) Du, H.; Haddon, R. C.; Krossing, I.; Passmore, J.; Rawson, J.M.; Schriver, M J., *Chem. Comm.*, **2002**, 1836.
- (35) Vela, S.; Mota, F.; Deumal, M.; Suizu, R.; Shuku, Y.; Mizuno, A.; Awaga, K.; Shiga, M.; Novoa, J. J.; Ribas-Arino, J. *Nat. Commun.* **2014**, *5*, 4411.
- (36) Luzon, J.; Campo, J.; Palacio, F.; McIntyre, G. J.; Rawson, J.M. *Polyhedron*, **2005**, *24*, 2579; (b) Deumal, M.; Rawson, J. M.; Goeta, A. E.; Howard, J. A. K.; Copley, R. C.; Robb, M. A.; Novoa, J. J. *Chem. Eur. J.*, **2010**, *16*, 2741.
- (37) (a) Bryan, C. D.; Cordes, A. W.; Haddon, R. C.; Hicks, R. G.; Kennepohl, D. K.; MacKinnon, C.D.; Oakley, R. T.; Palstra, T. T. M.; Perel, A. S.; Scott, S. R.; Schneemeyer, L. F.; Waszczak, J. V. *J. Am. Chem. Soc.*, **1994**, *116*, 1205. (b) Cordes, A. W.; Bryan, C. D.; Davis, W. M.; de Laat, R. H.; Glarum, S. H.; Goddard, J. D.; Haddon, R. C.; Hicks, R. G.; Kennepohl, D. K.; Oakley, R. T.; Scott, S. R.; Westwood, N. P. C. *J. Am. Chem. Soc.*, **1993**, *115*, 7232.
- (38) (a) Knapp, C.; Lork, E.; Gupta, K.; Mews, R.; *Z. Anorg. Allg. Chem.*, **2005**, *631*, 1640; (b) Clarke, C. S.; Pascu, S. I.; Rawson, J.M. *CrystEngComm*, **2004**, *6*, 79.
- (39) Fujita, W.; Awaga, K. *Science* **1999**, *286*, 261.
- (40) Brusso, J. L.; Clements, O. P.; Haddon, R. C.; Itkis, M. E.; Leitch, A. A.; Oakley, R. T.; Reed, R. W.; Richardson, J. F. *J. Am. Chem. Soc.*, **2004**, *126*, 14692.
- (41) Alberola, A.; Collis, R. J.; Humphrey, S. M.; Less, R. J.; Rawson, J.M.; *2006. Inorg. Chem.* **2006**, *45*, 1903.
- (42) Clarke, C. S.; Jornet-Somoza, J.; Mota, F.; Novoa, J. J.; Deumal, M. *J. Am. Chem. Soc.* **2010**, *132*, 17817.
- (43) Suizu, R.; Iwasaki, A.; Shuku, Y.; Awaga, K. *J.Mat.Chem.C*, **2015**, *3*, 7968.

To format double-column figures, schemes, charts, and tables, use the following instructions:

Place the insertion point where you want to change the number of columns

From the **Insert** menu, choose **Break**

Under **Sections**, choose **Continuous**

Make sure the insertion point is in the new section. From the **Format** menu, choose **Columns**

In the **Number of Columns** box, type **1**

Choose the **OK** button

Now your page is set up so that figures, schemes, charts, and tables can span two columns. These must appear at the top of the page. Be sure to add another section break after the table and change it back to two columns with a spacing of 0.33 in.

Table 1. Example of a Double-Column Table

Column 1	Column 2	Column 3	Column 4	Column 5	Column 6	Column 7	Column 8

Authors are required to submit a graphic entry for the Table of Contents (TOC) that, in conjunction with the manuscript title, should give the reader a representative idea of one of the following: A key structure, reaction, equation, concept, or theorem, etc., that is discussed in the manuscript. Consult the journal's Instructions for Authors for TOC graphic specifications.

